Testing tree crown economics with National Ecological Observatory Network

Yiting Fan

bgg3bj@virginia.edu

West Virginia University

Andrew J. Elmore

University of Maryland Center for Environmental Science

Brenden E. McNeil

West Virginia University

Article

Keywords: Broadleaf deciduous, Tree crown architecture, LiDAR, imaging spectroscopy, leaf angle, NIRv

Posted Date: August 12th, 2026

DOI: https://doi.org/10.21203/rs.3.rs-10529004/v1

Additional Declarations: No competing interests reported.

Abstract

Tree crown architecture—the three-dimensional density, distribution and inclination of leaves within a tree crown—modulates light interception and canopy function. Tree crown economic theory posits that crown architectural traits covary to describe a trade-off between light capture and atmospheric water demand, and influence crown-scale optical signals linked to photosynthesis. These hypotheses remain largely untested at the crown scale across environmental gradients. We combined tower-based photography with National Ecological Observatory Network airborne LiDAR and imaging spectroscopy to evaluate relationships among sunlit mean leaf angle, top rugosity, plant area index, accumulative plant area density in the upper 50% of the crown, and crown-scale near-infrared reflectance of vegetation (NIR_V) across nine eastern U.S. broadleaf deciduous sites and seven species. Crowns with more vertically-inclined leaves had a greater proportion of foliage distributed in the upper half of the crown, which were associated with lower crown-scale NIR_V. Interspecific patterns broadly matched known successional strategies, while within-species variation in *Liriodendron tulipifera* suggested possible acclimation of crown architecture along a moisture gradient. These results provide new cross-site evidence that remotely measurable crown traits are coordinated and linked to crown-scale reflectance, supporting future tests connecting crown economics to direct carbon and water flux measurements.

Introduction

Tree crown architecture — the three-dimensional density, distribution and inclination of leaves within a tree crown — plays a critical role in controlling light distribution and within-crown microclimate [1]. These architectural controls influence crown-scale light interception, heat exchange, and spectral reflectance, and may therefore mediate physiological processes such as photosynthesis and evapotranspiration that strongly drive ecosystem responses to global change [2, 3, 4]. As part of their adaptive and acclimatory strategies, trees have long been known to exhibit diverse crown architectures that reflect both evolutionary history and plastic responses to environmental variability and competition [5, 1]. However, the mechanistic basis behind this architectural diversity remains poorly documented and quantified at the essential crown scale, limiting our ability to fully integrate crown architecture into remote sensing models useful for predicting forest functioning [6, 7].

Trait-based and metabolic scaling frameworks already invoke economic trade-offs between architecture and function to explain emergent ecosystem properties [8, 9]. At the leaf scale, co-varying architectural and chemical traits such as leaf mass per area and leaf nitrogen content predict photosynthetic and respiratory capacities under the leaf economics spectrum [10]. At the ecosystem scale, canopy structural metrics such as leaf area index and canopy height similarly predict ecosystem productivity and energy balance [2]. Recent work has suggested that crown architectural features such as crown size can influence radial growth and drought resilience [11, 12]. Nevertheless, while robust architecture-function linkages exist at the leaf and the ecosystem scales, the essential organismal scale of the individual tree crown remains a critical gap, largely due to the lack of standardized characterization of

crown architecture [13] and challenges in traditional measurement across suitable biogeographic gradients [4, 6].

Tree crown economic theory proposes that key aspects of crown architecture can be defined through a suite of co-varying crown traits that describe the inclination, density, and distribution of leaves within a crown [6]. Among these traits, mean leaf inclination angle (MLA) — the average angle between the leaf normal and the zenith [14] — plays a central role in controlling projected leaf area, crown openness, light penetration, and spectral reflectance [15, 7]. MLA has been shown to respond to heat and drought stress, and genetic studies have identified regulatory pathways underlying variation in leaf angle, underscoring its adaptive importance in dynamic light environments and dense canopies [16]. The density, distribution, and inclination of leaves collectively shape patterns of sunlit and shaded foliage, affecting radiative transfer, photosynthetically active radiation, and the exchange of heat and gases within and around crowns [17, 18]. Measuring traits such as MLA has been revolutionized by modern techniques such as LiDAR and photographic analysis of leveled profile images, overcoming limitations of labor-intensive, time-consuming traditional methods [19, 20]. While terrestrial LiDAR enables rapid and non-destructive measurement of leaf angles using high-resolution 3-D point clouds, photographic analysis offers a cost-effective alternative that allows high-frequency temporal tracking of leaf angles [6].

Advancements in LiDAR imaging have enabled measurements of other crown architectural traits. For instance, crown surface rugosity (R_t), defined as the standard deviation of canopy height, provides a complementary descriptor of outer crown shape and roughness that can influence light penetration and microclimate down the canopy [21]. Voxelizing LiDAR point clouds enables three-dimensional quantification of plant area density (PAD). By vertically summing PAD profiles within field-delineated tree crowns, researchers can obtain a measure of foliage density at each height strata within the crown [22]. Then, summing the accumulative PAD from the crown top to a defined height (e.g. the upper 50% of the canopy height, $APAD_{50}$) characterizes how foliage is distributed along the vertical light gradient, defining the fundamental crown architecture trade-off of growing out (low $APAD_{50}$) versus up (high $APAD_{50}$). Finally, summing PAD through the entire crown yields plant area index (PAI), a measure of overall crown density.

Together, potential traits like MLA, R_t, $APAD_{50}$, and PAI can capture several important dimensions of crown architecture. These measurable crown traits are hypothesized to co-vary and sort species along an economic spectrum of crown architectures, reflecting architectural-functional trade-offs among light capture, construction costs, and exposure to atmospheric water demand [6]. At one end of this spectrum, a hypothesized “dome” ideotype is characterized by horizontally inclined leaves (low MLA) and horizontally-distributed (low $APAD_{50}$), dense foliage (high PAI) that maximizes light interception and casts deep shade on competitors — traits that may be particularly advantageous for late-successional species in mesic environments [15, 23]. In contrast to “dome” ideotype architectures, many canopy-emergent trees or trees in drier or high-light environments are hypothesized to adapt a “tower” ideotype architecture of top-heavy crowns with vertically inclined leaves [5], facilitating light penetration through multiple crown layers and reducing effective radiation load on individual leaves [1, 24, 6].

Critically, crown architecture determines the crown's light-scattering properties, which are uniquely captured by spectral reflectance in the near-infrared (NIR) wavelengths [25, 17]. In particular, the Near-Infrared Reflectance of Vegetation (NIR_v) has emerged as a powerful spectral metric, because it is not only highly correlated with the fraction of absorbed photosynthetically active radiation (fPAR) by green vegetation, but also effectively isolates the NIR signal from sunlit leaves and removes confounding effects of non-photosynthetic elements such as shadows or soil [26]. Physiologically, NIR_v tracks changes that are tightly linked to photosynthetic capacity: increases in total leaf area or changes in leaf angle that optimize light capture are often, though not universally, accompanied by increases in canopy photosynthesis and gross primary production (GPP) [27, 28, 6]. The mechanistic relationship is strongest under less-stressed, sunlit conditions but can be uncoupled during periods of physiological down-regulation, as NIR_v largely reflects the optical, not biochemical, state of the canopy [20, 28]. This makes NIR_v a widely used proxy for vegetation functional capacity across space and time for mesic broadleaf deciduous forests [26, 28, 29]. Fine-scale NIR_v measurements thus offer an unparalleled opportunity to detect meaningful spatial patterns in the economic spectrums of crown architecture and linked ecological processes.

Here, we partner with the National Ecological Observatory Network (NEON) to test crown economic theory through tower-based and airborne remote sensing data collections. By offering *in-situ* measurements and high-resolution LiDAR and imaging spectroscopy from the airborne observation platform (AOP), NEON allows consistent measurements of tree crown architectural traits and crown-scale reflectance across diverse biogeographic and climatic settings characteristic of forests across the eastern United States. We collected new observations and combined these with standard NEON data from nine broadleaf deciduous sites to quantify crown traits and NIR_v across diverse tree species. We quantify: (1) sunlit MLA from new NEON tower-based photography, (2) other crown traits (e.g. PAI, $APAD_{50}$) from NEON AOP LiDAR extracted from field-delineated crowns, and (3) crown-scale NIR_v from AOP spectrometer data. We combine these data to evaluate two key hypotheses of crown economic theory: (1) measurable crown traits will co-vary to describe an economic trade-off of light capture versus exposure to atmospheric water demand, and (2) crown traits can predict crown-scale NIR_v [6].

Results

Species variability in crown architectural traits and NIR_v

Species-associated differences explained between 23–62% of the total variance in tree height, MLA, $APAD_{50}$, and NIR_v (Fig. 1). We observed that *Liriodendron tulipifera* and *Betula alleghaniensis* exhibited more vertical leaf angles (higher MLA), more vertical in their leaf distribution (higher $APAD_{50}$), and lower NIR_v. *Acer saccharum* had the most horizontal leaf angles (lowest MLA), more horizontal crowns (lower $APAD_{50}$), and much higher NIR_v. However, R_t or PAI did not differ significantly among species, indicating

limited species-associated variation in outer-crown surface complexity and crown density in our measurements.

Covariations among crown architectural traits and NIR

We found evidence for coordinated variation between two crown architectural traits: site-species combinations with more top-heavy crowns (higher $APAD_{50}$; e.g., *L. tulipifera*) also tended to have more vertically inclined leaves (higher MLA) (Figs. 1 and 2a). That is, crowns accumulating more plant area in the top half of the crown were consistently the crowns with more vertical leaves at the sunlit treetop. Support for the co-variation of crown architectural traits was limited to the correlation between MLA and $APAD_{50}$, as we did not observe significant co-variation of MLA with other possible crown traits, such as R_t or crown density (PAI).

Table 1

Study sites and the thirteen site–species combinations for which tower-based leaf-angle measurements were paired with NEON airborne crown traits and NIR_v measurements. Sites are ordered by increasing site moisture index, calculated as mean annual precipitation divided by potential evapotranspiration [55].

Site, State	Lat, Lon	MAP/PET Index	Measured Tree Species	Crown Base Height (m)	AOP Dates	MLA Dates
UKFS, KS	39.04,-95.19	0.68	*Carya ovata*	5	6/9/2022	6/8/2023
SERC, MD	38.89,-76.56	0.81	*Carya ovata* *Liriodendron tulipifera*	10	8/11/2021	8/9/2021; 8/16/2021
SCBI, MD	38.89,-78.14	0.85	*Liriodendron tulipifera*	10	8/12/2021	8/8/2021; 8/14/2021
TREE, WI	45.49,-89.59	0.88	*Acer saccharum*	9	6/18/2022	6/18/2022
MLBS, VA	37.38,-80.52	0.91	*Acer rubrum*	10	6/17/2021	7/28/2021
ORNL, TN	35.96,-84.28	0.95	*Quercus montana* *Quercus velutina* *Liriodendron tulipifera*	10	5/11/2018	7/26/2021; 7/29/2021
UNDE, MI	46.23,-89.54	0.96	*Acer saccharum*	8	6/20/2022; 6/24/2022	6/18/2022; 6/25/2022
GRSM, TN	35.69,-83.50	1.20	*Liriodendron tulipifera*	14	6/18/2021; 6/26/2021	7/30/2021; 7/31/2021
BART, NH	44.06,-71.29	1.31	*Acer rubrum* *Betula alleghaniensis*	9	8/19/2022; 8/20/2022	8/16/2022; 8/20/2022

$APAD_{50}$ and MLA were both negatively associated with crown-scale NIR_v, although the model containing MLA explained 32% more variation in NIR_v than the model containing $APAD_{50}$ (Fig. 2). The leave-one-out analyses showed that the MLA–$APAD_{50}$ (adjusted R^2 0.18–0.46) and MLA–NIR_v (adjusted R^2 0.31–0.52) relationships were directionally consistent across all iterations and not driven by any single site-species combination (Supplementary Table S1). The $APAD_{50}$–NIR_v relationship remained negative but was less stable across iterations (adjusted R^2 = 0.03–0.33).

For *L. tulipifera* present at four of the nine NEON sites, crowns from more mesic sites showed elevated NIR_v (Table 2). MLA and $APAD_{50}$ showed similar directional but non-significant trends with site moisture, with more mesic sites tending to have more horizontally inclined leaves (lower MLA) and more horizontally distributed crowns (lower $APAD_{50}$).

Table 2
Within-species variation in *Liriodendron tulipifera* across four sites. Pearson correlation coefficients relate crown traits to the site moisture index (MAP/PET). All P values are two-sided.

Trait	n	r	p-value	F(1, 2)
MLA	4	-0.86	0.143	5.51
PAI	4	-0.68	0.316	1.76
R_t	4	-0.87	0.135	5.95
$APAD_{50}$	4	-0.8	0.199	3.57
MAXCH	4	**-0.94**	0.062	14.61
NIR_v	4	**0.9992**	0.001	1270.31

Discussion

Our results provide cross-site evidence that some predicted dimensions of tree crown economic theory can be detected using coordinated tower-based and airborne remote-sensing observations. Species-associated differences in crown traits and NIR_v broadly aligned with hypothesized “tower” and “dome” architectural ideotypes [6], supported connections between crown architecture and established ecological classifications such as shade tolerance [37] and moisture niche preference [38], and illustrated how remotely measurable traits may be used to identify species that broadly occupy different positions along a crown economic spectrum [6].

Early-successional or canopy-emergent species such as *L. tulipifera* and *B. alleghaniensis* exhibited traits consistent with a “tower” ideotype, including more vertically inclined leaves (higher MLA, Fig. 1a) and more top-heavy crowns (higher $APAD_{50}$, Figs. 1b and 2a), which also tended to be associated with lower NIR_v (Figs. 1 and 2). More vertical leaf angles can reduce direct radiation load on individual leaves, limit overheating, and provide partial shading within the crown, allowing upper sunlit leaves to operate closer to their light saturation points while avoiding excessive heat [5, 30, 3, 31]. Such architectures are consistent with known hormonal and genetic controls of leaf angle, including pathways involving brassinosteroids, auxin transport, auxin-phytochrome crosstalk that underlie shade-avoidance strategy, as well as regulatory genes that modulate lamina inclination to balance light interception and self-shading in dense canopies [32, 16]. By distributing a greater proportion of leaves to upper, sunlit

positions, and orienting those leaves more vertically, these “tower” species may promote deeper light penetration through multi-layered crowns and support rapid vertical growth in high-light environments [31].

In contrast, several species in our dataset exhibited crown traits more characteristic of the “dome” ideotype that is thought to be sub-optimal, but most adaptive in mesic, late-successional forest environments [6]. In particular, *A. saccharum*, a relatively shade-tolerant and late-successional species, had the most horizontal leaf angles (lowest MLA, Fig. 1a), and was among the species with leaves distributed in the least vertical, rugose fashion relative to the vertical light gradient at each site (lower $APAD_{50}$, Fig. 1b). Horizontal leaf and branch arrangements may confer advantages in late-successional environments by increasing interception of diffuse light and casting deeper and more persistent shade on less shade-tolerant competitors, suppressing their growth and recruitment [1, 25, 33]. This architecture aligns with a shade-tolerance syndrome where leaves with high chlorophyll content and low light compensation points are arranged to capture light efficiently in closed-canopy, light-limited stands while maintaining relatively low photosynthetic saturation irradiances [28, 34, 35]. A dense and horizontal foliage arrangement can also increase photon-leaf interaction probability in the upper canopy, enhancing multiple scattering and providing a potential mechanism through which canopy architecture contributes to higher canopy NIR reflectance [36, 25]. Consistent with this interpretation, our observation of higher NIR_v values of *A. saccharum* (Fig. 1f) suggests that its crown architecture may contribute to stronger crown-scale optical signals associated with photosynthetic light capture [28]. Crown architectures that maximize intercepted light also, by necessity, expose a larger projected leaf area. This architectural exposure could potentially increase the risk of water stress in drier conditions unless buffered by efficient physiological regulation, such as active stomatal closure and favorable hydraulic traits affecting xylem vulnerability and capacitance [41, 42, 43, 44]. The need to balance light acquisition with water conservation raises the question of whether crown architecture varies predictably along site moisture gradients within species.

The differences observed among the four *L. tulipifera* sites provide preliminary evidence that crown architecture and crown-scale reflectance may vary along persistent climatic moisture gradients within a species. *L. tulipifera* at more mesic sites showed elevated NIR_v (Table 2), while MLA and $APAD_{50}$ showed non-significant trends toward more horizontally inclined leaves (lower MLA, $r = -0.86$, $F(1,2) = 5.51$) and more horizontal crowns (lower $APAD_{50}$, $r = -0.80$, $F(1,2) = 3.57$). While this analysis was limited to four sites, the direction of the observed trends is consistent with the expectation that crown architectures in drier sites may shift toward more vertically inclined leaves and more vertically distributed foliage, traits that can reduce direct radiation load and potentially moderate heat and water stress [45, 24, 46]. Vertically inclined leaves can reduce leaf temperature and transpirational water demand by reducing the leaf area directly orthogonal to midday irradiance and high vapor pressure deficit, while more vertically distributed crowns may further enhance convective cooling by improving airflow around leaves [45, 24, 46]. This coordinated architectural adjustment in drier environments could potentially help the tree maintain favorable hydraulic conditions and avoid catastrophic xylem cavitation when water is limiting

[42, 44]. In contrast, in more mesic sites, more horizontal leaf angles and less vertically distributed crowns coincided with higher NIR_v, suggesting that the architecture of *L. tulipifera* may adjust toward greater light interception in locations where water availability is relatively abundant and hydraulic constraints are minimal.

The site-level variation observed in *L. tulipifera* may reflect a combination of persistent ecotypic differences among populations, local acclimation to moisture regimes, and/or short-term responses such as selective leaf shedding to reduce transpirational load during dry conditions [11, 47]. At the branch scale, increased leaf inclination angle is a well-documented drought avoidance strategy that can reduce absorbed energy load, water loss and heat stress while maintaining photosynthetic efficiency by reducing the absorbed energy load [45, 24, 48, 46]. These observations suggest that adjustments in branch- and crown-scale architecture can provide a plastic and effective means by which trees navigate the inherent trade-off between maximizing light interception and minimizing exposure to atmospheric water demand [24]. However, the small number of *L. tulipifera* site observations here prevents us from distinguishing plasticity from population-level or site-level differences. Future studies combining repeated measurements, common-garden comparisons, or within-site moisture contrasts would be needed to test whether these crown architectural variations persist to reflect true acclimation.

Strong inter- and intraspecific variability reinforced the architectural coordination between MLA and $APAD_{50}$, and demonstrated their collective ability to predict crown-scale NIR_v (Fig. 2). Although the correlation among MLA and $APAD_{50}$ and the limited sample size of the combined dataset precluded us from fully disentangling their individual effects on NIR_v, the fact that MLA alone explained 32% more variance than $APAD_{50}$ suggests that leaf inclination is the stronger architectural factor influencing spectral reflectance at the crown scale. Mechanistically, the convergent traits of MLA and $APAD_{50}$ both affect NIR_v by collectively regulating light penetration and scattering dynamics within the crown [25, 36]. As theorized decades ago [5], more vertical leaf angles can facilitate deeper photon transmission into a more layered and vertically distributed (higher $APAD_{50}$) crown, reducing light interception at the outer surface and increasing the probability of multiple scattering among leaves within vertically stratified crowns. Conversely, crowns with more horizontally inclined leaves intercept a larger fraction of incoming radiation near the crown surface, producing a stronger single-scattering surface signal with less deep penetration [17]. These patterns are consistent with the idea that leaf angle and related fine-scale architectural properties, such as clumping and within-shoot scattering, are likely among the strongest determinants of canopy NIR reflectance [49, 17, 36]. These properties are thus promising metrics for trait-based, remotely sensed assessments of crown architecture, and our observed trait coordination provides an empirical foundation for future work that explicitly links crown economics to direct carbon and water flux measurements to evaluate their functional consequences.

Limitations and future directions

Our tower-based measurements of sunlit leaves reinforced the central role of outer crown surface in regulating canopy NIR reflectance [17]. Given this role, the lack of a clear relationship between NIR_v and crown shape (crown rugosity, R_t) was somewhat surprising. While R_t and PAI did not differ significantly by species, both metrics are particularly sensitive to LiDAR pulse density [39] and are likely influenced by large variation in disturbance and age-related forest dynamics across the nine NEON sites [40]. PAI and R_t were previously found to differ among species using higher-resolution portable LiDAR data collected in even-aged plantation settings with more similar disturbance regimes [6]. In contrast, the NEON AOP data used here represent naturally structured forests across multiple sites, where variation in stand history, crown overlap, LiDAR sampling geometry, along with the strong random nature of PAI crown measurements may confound our ability to detect species-level differences in crown density or outer crown rugosity. While MLA and $APAD_{50}$ were better resolved in this dataset, finer-scale properties such as foliage clumping and leaf-angle distributions may exert stronger controls on NIR_v than coarse measures of crown shape [39]. Fully disentangling the roles of crown density, outer-crown shape, and fine-scale foliage organization will likely require LiDAR data with substantially higher pulse density than those currently available from the NEON AOP.

Translating LiDAR returns into PAI and $APAD_{50}$ required assuming a constant light-extinction coefficient, *k*, across species and sites. In reality, *k* varies with crown-scale (e.g., branching patterns), branch-scale (e.g., leaf angle and clumping), and leaf-scale (e.g., leaf thickness) properties [17]. We used a fixed value to maintain methodological consistency across sites, and the resulting PAI and related metrics derived from a fixed *k* should therefore be interpreted as standardized structural indices rather than absolute measurements of plant area. Higher-density terrestrial, mobile, or unoccupied-aerial-system LiDAR data, combined with methods that explicitly account for leaf angle and clumping, could improve the biological interpretation of these traits.

Temporal variability in crown architecture remains a key frontier for linking crown economics with seasonal and/or annual canopy function. Crown traits such as $APAD_{50}$ may change seasonally as trees selectively shed leaves or adjust foliage distributions in response to seasonal or episodic drought [47]. Leaf angles can also vary phenologically in ways that directly influence NIR_v [50, 6]. Continuous concurrent time-series measurements of crown architectural traits, NIR_v, and physiological fluxes could thus help distinguish persistent architectural strategies from short-term acclimatory responses.

Our findings may have practical value for forest monitoring and silviculture under climate change. Interspecific differences in MLA, $APAD_{50}$, and associated optical signatures such as NIR_v could inform climate-adaptive management by helping identify crown architectures that are more compatible with projected shifts in light and moisture regimes, and by guiding species selection and stand composition aimed at maintaining productivity and hydraulic safety in future climates. Because these traits and their associated NIR signals can be observed remotely, they may provide a practical basis for monitoring whether managed stands are shifting toward more drought-tolerant crown architectures through time, and for evaluating the architectural consequences of alternative management strategies. Building on

recent evidence that leaf angle and other crown traits are under genetic control in diverse species, for example [51, 16], linking crown traits and canopy reflectance to genomic and transcriptomic data offers a promising pathway to identify the regulatory pathways underlying crown architecture. Such integrative studies could help pinpoint genes and regulatory networks associated with “tower” versus “dome” strategies, thereby informing assisted migration, selective breeding, and other silvicultural interventions to promote climate-resilient crown architectures. We also suggest linking tree crown economic theory to complementary frameworks such as leaf economics and functional diversity [22]. Together with leaf traits, crown traits could provide a powerful basis for refining and testing crown-scale models of photosynthesis and resource allocation. Such mechanistic approaches are crucial for improving predictions of how diverse forest ecosystems will acclimate and respond to future shifts in resource availability under global change scenarios.

Finally, our data highlight great potential of broad-scale open observation networks like NEON for testing new hypotheses and theory. By continuing to co-locate AOP and field observations and maintaining open data archives, NEON remains a vital observatory with tremendous potential for testing whether crown architectural patterns generalize across species, sites, and environmental gradients at continental scales. While our test relied on a bespoke sample of high-quality tower-based leaf angle observations and field-delineated crowns for extracting AOP data, emerging machine learning tools are now integrating NEON LiDAR and spectroscopy to assess species and architectural diversity across millions of crowns [52]. These advances offer opportunities to expand crown economic analyses beyond our limited site-species combinations evaluated here.

Conclusion

Trait-based approaches offer a useful framework for characterizing how ecophysiological trade-offs in tree crown architecture may shape tree functional performance under changing environments. Using new and standard NEON data, we found support for coordinated variation between measurable traits of sunlit mean leaf angle (MLA) and vertical leaf distribution ($APAD_{50}$) across a moisture gradient, suggesting that these traits can define an important axis of crown architectural trade-off among light capture versus water use efficiency. We also found that MLA and $APAD_{50}$ were associated with crown-scale NIR_v, indicating that crown architecture contributes to remotely sensed optical signals linked to light capture. By documenting that these crown traits and NIR_v vary in a coordinated way across species and sites spread across eastern U.S. broadleaf deciduous forests, this study lays a foundation for incorporating tree crown economic theory into remote sensing-based assessments of forest responses to global change.

Methods

Study sites and species

Based on the availability (as of June 2025) of NEON field-delineated crown polygons, we selected nine sites spanning a strong climate gradient representative of the North American broadleaf deciduous forest biome (Table 1). We focused on seven common native broadleaf deciduous tree species that occurred across one or more sites (Table 1), allowing us to examine interspecific co-variation in crown traits and crown-scale reflectance across contrasting environments. We also leveraged the climate gradient to assess site-level variation in the most common species in our sample, *L. tulipifera*, which occurred at four of the nine sites. For this subset, we examined how crown traits and crown-scale NIR_v varied with a site-level moisture index (MAP/PET) derived from long-term gridded climatologies (Table 1). We used this ratio as an index of site-level climatic moisture availability to compare persistent differences in site water balance, with higher values indicating relatively more mesic conditions. Because crown architectural traits likely integrate tree responses over multiple weeks to decades, long-term climate metrics like MAP/PET provide a more appropriate measure of the moisture regime that shape persistent differences in crown architecture than instantaneous meteorological conditions.

Crown traits from LiDAR

We extracted crown architectural traits from NEON AOP discrete-return LiDAR data (DP1.30003.001). We filtered the LiDAR point clouds extracted from quality-checked crown polygons (Supplementary Fig. S1) and computed common architectural metrics using 1-m^3 voxelated data using a Beer-Lambert-type gap fraction model with a light extinction coefficient (*k*) of 0.5 across all sites [21, 22]. We used a fixed *k* to maintain methodological consistency across sites and species, while recognizing that *k* can vary with leaf angle distribution, foliage clumping, branching architecture, and leaf optical properties. We therefore interpret PAI and $APAD_{50}$ as standardized LiDAR-derived structural indices rather than absolute measurements of plant area. We focus here on three candidate crown traits describing leaf density and distribution: R_t, PAI, and $APAD_{50}$. We used R_t to describe the variability of the outer crown surface [22]. We computed plant area index (PAI) to represent crown density, which was the column sum of plant area density (PAD) [53, 22]. Here, PAD is defined as the number of LiDAR plant returns relative to all LiDAR pulses within each 1-m^2 vertical column [22]. Furthermore, the accumulative PAD from the crown top to a defined height (e.g. the upper 50% of the canopy height, $APAD_{50}$) characterizes how foliage is distributed along the vertical light gradient, defining the crown architectural trade-off of growing out (low $APAD_{50}$) versus up (high $APAD_{50}$). $APAD_{50}$ increases in top-heavy crowns that emerge from the canopy, typically with leaves distributed in multiple vertical layers [5]. Computational details of each trait are provided in Supplementary Information.

Near-infrared reflectance of vegetation

We used AOP imaging spectrometer data to compute spectral indices for each delineated crown across the sites. For this analysis, we selected NIR_v over other vegetation indices (e.g., NDVI) because of its sensitivity to sunlit vegetation reflectance and its previously documented relationships with canopy structure, fPAR, and photosynthetic activity. Due to data availability at the time of processing, we used

two imagery products: for 2022, we used the new bidirectional reflectance (DP3.30006.002), which corrects for angular effect in illumination and viewing geometry; for prior years, we used the older directional product (DP1.10026.001), which does not include this angular correction. We computed NIR_v as:

$$NIR_v = NIR \times NDVI \text{ [26] (1)}$$

$$NDVI = \frac{(NIR-RED)}{(NIR+RED)} \text{ [54] (2)}$$

where NIR is the near-infrared reflectance (band 90, central wavelength ≈ 829nm), and RED is the red reflectance (band 58, ≈ 669nm). To evaluate potential impact of using different products, we compared NIR_v values derived from the two products for three sites where both products were available (Supplementary Fig. S2). This comparison suggested limited systematic differences between products at those sites, likely because of within-crown pixel averaging and the ratio-based nature of NIR_v. However, product differences remain a source of uncertainty because product type is partly confounded with year and site in the full dataset.

Crucially, because NIR_v is influenced by view geometry, background reflectance, and atmospheric conditions, especially when comparing different years and products, we focus on relative differences in NIR_v among crowns, species, and sites and on its co-variation with the crown traits. This approach allows us to interpret NIR_v as a crown-scale optical metric that integrates information about crown architecture and photosynthetic activity, rather than as a direct, absolute measurement of physiological fluxes such as carbon assimilation or evapotranspiration.

Mean leaf angle

Through an agreement with NEON, we installed two time-lapse cameras at each NEON tower, mounted level to sunlit treetops, and set to collect hourly photos throughout 2021–2023 growing seasons. When possible, we measured leaf angles from images taken at solar noon (1 pm) on an approximately weekly basis, producing a larger data archive used separately for analyzing leaf angle phenology. In several instances, camera malfunctions or disturbance to the crowns in the time-lapse camera field of view precluded making quality leaf angle measurements at times when AOP overflights occurred (e.g. at GRSM, SCBI and SERC in 2022, see Supplementary Fig. S2). For this study, we used all available measurements from quality time-lapse camera images that coincided with an AOP overflight at each site (Table 1), or from phenologically representative dates when no direct match was available at two sites (ORNL and UKFS). We screened images to avoid weather-related artifacts (e.g., wind, fog, rain), substituting poor images with those taken within ± 2 days. Following established protocols [19, 20], we selected 75 leaves to measure per species per site. We selected leaves that were oriented in the plane of the image, and recorded (x, y) image coordinates of the petiole and tip, from which we calculated leaf angle. We then computed MLA for each site-species combination from these leaf-level measurements.

Statistical analysis

We compiled a summary dataset of 13 site-species combinations (Supplementary Table S2) where MLA could be matched with AOP-derived crown trait metrics (PAI, $APAD_{50}$, R_t and NIR_v). We used reduced major axis regressions (RMA) to evaluate trait co-variation and univariate regressions to assess trait effects on NIR_v. Given the small number of site-species combinations, we also conducted leave-one-out sensitivity analyses for the primary relationships by refitting each model after sequentially removing one site-species combination. This was to assess whether the observed relationships were strongly dependent on any single site-species combination. We then evaluated interspecific variability in the crown traits and NIR_v using one-way ANOVA with Tukey's HSD post-hoc tests. For *L. tulipifera* present at four sites, we used linear regression to test whether site moisture (MAP/PET; Table 1) was predictive of site-level variability in crown traits or NIR_v.

All reported P values are two-sided. Statistical sample sizes and the associated measures of centre and uncertainty are reported in the figures, tables and supplementary data. Reduced major axis regression was used for trait–trait relationships because both variables were measured with uncertainty; ordinary least-squares regression was used when predicting NIRv from crown traits.

Declarations

Competing interests:

The authors declare no competing interests.

Funding:

This work was supported by the U.S. National Science Foundation's Division of Environmental Biology, Macrosystems Biology and NEON-Enabled Science program (award no. 2106080), through funding awarded to Brenden E. McNeil and Andrew J. Elmore.

Author Contribution

Y.F. processed the data, performed the analyses and drafted the manuscript. B.E.M. and A.J.E. conceived the theoretical framework and study design. Y.F. and B.E.M. collected the project data and supervised the undergraduate researchers who performed the leaf-angle measurements. All authors interpreted the results, revised the manuscript and approved the final version.

Acknowledgement

This study was supported by a National Science Foundation (NSF) MacroSystems Biology & NEON-Enabled Science (MSB-NES) program grant (#2106080) awarded to BEM and AJE. We are grateful to the

National Ecological Observatory Network (NEON) for their collaboration — particularly the AOP team and domain technicians who assisted with the installation and maintenance of our leaf angle time-lapse cameras on NEON towers. We thank Stephen Guinn and Burch Fisher for excellent data management and advice. We are also indebted to a dedicated team of undergraduate researchers: Wiliam Brown, Ethan Cade, Abbie Carter, Connor Channels, Andrew Indomenico, Grant Keefer, Liz Murtha, Lydia Nicolai, Mason Powell, and Nikki Vilasuso. Their contributions were supported by an NSF Research Experiences for Undergraduates (REU) grant supplement, the West Virginia University (WVU) Summer Undergraduate Research Experience Program, and the WVU Research Apprenticeship Program.

Data Availability

The datasets generated and analyzed in this study were deposited into the Environmental Data Initiative and are available at the following URL:
https://doi.org/10.6073/pasta/f022939a1245a646336ff48946026ea8.

References

1. Givnish, T. J. Adaptation to sun and shade: a whole-plant perspective. *Aust J. Plant. Physiol.* **15**, 63–92. https://doi.org/10.1071/PP9880063 (1988).
2. Fahey, R. T. et al. Defining a spectrum of integrative trait-based vegetation canopy structural types. *Ecol. Lett.* **22**, 2049–2059. https://doi.org/10.1111/ele.13388 (2019).
3. Falster, D. S. & Westoby, M. Leaf size and angle vary widely across species: what consequences for light interception? *New. Phytol*. **158**, 509–525. https://doi.org/10.1046/j.1469-8137.2003.00765.x (2003).
4. Norman, J. M. & Campbell, G. S. Canopy structure in Plant Physiological Ecology: Field Methods and Instrumentation 301–325 (Springer, 1989); https://doi.org/10.1007/978-94-009-2221-1_14
5. Horn, H. S. *Adaptive Geometry of Trees* (Princeton University Press, 1971). https://doi.org/10.2307/j.ctvx5w9x8
6. McNeil, B. E. et al. Tree crown economics. *Front. Ecol. Environ.* **21**, 40–48. https://doi.org/10.1002/fee.2588 (2023).
7. Yang, X. et al. Leaf angle as a leaf and canopy trait: rejuvenating its role in ecology with new technology. *Ecol. Lett.* **26**, 1005–1020. https://doi.org/10.1111/ele.14215 (2023).
8. Craine, J. M. *Resource Strategies of Wild Plants* (Princeton University Press, 2009). https://doi.org/10.1515/9781400830640
9. Enquist, B. J., West, G. B. & Brown, J. H. Extensions and evaluations of a general quantitative theory of forest structure and dynamics. Proc. Natl Acad. Sci. USA 106, 7046–7051; (2009). https://doi.org/10.1073/pnas.0812303106

10. Wright, I. J. et al. The worldwide leaf economics spectrum. *Nature* **428**, 821–827. https://doi.org/10.1038/nature02403 (2004).
11. Kröner, K. et al. Influence of crown morphology and branch architecture on tree radial growth of drought-affected Fagus sylvatica L. *Ecosyst.* **11**, 100237. https://doi.org/10.1016/j.fecs.2024.100237 (2024).
12. Verbeeck, H. et al. Time for a plant structural economics spectrum. *Front. Glob Change*. **2**, 43. https://doi.org/10.3389/ffgc.2019.00043 (2019).
13. Disney, M. Terrestrial LiDAR: a three-dimensional revolution in how we look at trees. *New. Phytol*. **222**, 1736–1741. https://doi.org/10.1111/nph.15517 (2019).
14. Ross, J. *The Radiation Regime and Architecture of Plant Stands* (Springer, 1981). https://doi.org/10.1007/978-94-009-8647-3
15. Ellsworth, D. S. & Reich, P. B. Canopy structure and vertical patterns of photosynthesis and related leaf traits in a deciduous forest. *Oecologia* **96**, 169–178. https://doi.org/10.1007/BF00317729 (1993).
16. Tian, J. et al. Maize smart-canopy architecture enhances yield at high densities. *Nature* **632**, 576–584. https://doi.org/10.1038/s41586-024-07669-6 (2024).
17. Béland, M. & Kobayashi, H. Drivers of deciduous forest near-infrared reflectance: a 3D radiative transfer modeling exercise based on ground lidar. *Remote Sens. Environ.* **302**, 113951. https://doi.org/10.1016/j.rse.2023.113951 (2024).
18. Fotis, A. T. & Curtis, P. S. Effects of structural complexity on within-canopy light environments and leaf traits in a northern mixed deciduous forest. *Tree Physiol.* **37**, 1426–1435. https://doi.org/10.1093/treephys/tpw124 (2017).
19. Ryu, Y. et al. How to quantify tree leaf area index in an open savanna ecosystem: a multi-instrument and multi-model approach. *Agric. Meteorol.* **150**, 63–76. https://doi.org/10.1016/j.agrformet.2009.08.007 (2010).
20. Raabe, K., Pisek, J., Sonnentag, O. & Annuk, K. Variations of leaf inclination angle distribution with height over the growing season and light exposure for eight broadleaf tree species. *Agric. Meteorol.* **214**, 2–11. https://doi.org/10.1016/j.agrformet.2015.07.008 (2015).
21. Atkins, J. W. et al. Quantifying vegetation and canopy structural complexity from terrestrial LiDAR data using the forestr R package. *Methods Ecol. Evol.* **9**, 2057–2066. https://doi.org/10.1111/2041-210X.13061 (2018).
22. Kamoske, A. G., Dahlin, K. M., Stark, S. C. & Serbin, S. P. Leaf area density from airborne LiDAR: comparing sensors and resolutions in a temperate broadleaf forest ecosystem. *Ecol. Manage.* **433**, 364–375. https://doi.org/10.1016/j.foreco.2018.11.017 (2019).
23. Walters, M. B. & Reich, P. B. Are shade tolerance, survival, and growth linked? Low light and nitrogen effects on hardwood seedlings. *Ecology* **77**, 841–853. https://doi.org/10.2307/2265505 (1996).
24. Gamon, J. A. & Pearcy, R. W. Leaf movement, stress avoidance and photosynthesis in Vitis californica. *Oecologia* **79**, 475–481. https://doi.org/10.1007/BF00378664 (1989).

25. Ollinger, S. V. Sources of variability in canopy reflectance and the convergent properties of plants. *New. Phytol*. **189**, 375–394. https://doi.org/10.1111/j.1469-8137.2010.03536.x (2011).
26. Badgley, G., Field, C. B. & Berry, J. A. Canopy near-infrared reflectance and terrestrial photosynthesis. *Sci. Adv.* **3**, e1602244. https://doi.org/10.1126/sciadv.1602244 (2017).
27. Dechant, B. et al. Canopy structure explains the relationship between photosynthesis and sun-induced chlorophyll fluorescence in crops. *Remote Sens. Environ.* **241**, 111733. https://doi.org/10.1016/j.rse.2020.111733 (2020).
28. Baldocchi, D. D. et al. Outgoing near-infrared radiation from vegetation scales with canopy photosynthesis across a spectrum of function, structure, physiological capacity, and weather. *J. Geophys. Res. Biogeosci*. **125** https://doi.org/10.1029/2019JG005534 (2020). e2019JG005534.
29. Dechant, B. et al. NIRVP: a robust structural proxy for sun-induced chlorophyll fluorescence and photosynthesis across scales. *Remote Sens. Environ.* **268**, 112763. https://doi.org/10.1016/j.rse.2021.112763 (2022).
30. McMillen, G. G. & McClendon, J. H. Leaf angle: an adaptive feature of sun and shade leaves. *Bot. Gaz.* **140**, 437–442. https://doi.org/10.1086/337110 (1979).
31. Hikosaka, K., Kumagai, T. O. & Ito, A. Modeling canopy photosynthesis. *J. Plant. Res.* **129**, 239–268. https://doi.org/10.1007/s10265-016-0824-1 (2016).
32. Smith, H. & Whitelam, G. C. The shade avoidance syndrome: multiple responses mediated by multiple phytochromes. *Plant. Cell. Environ.* **20**, 840–844. https://doi.org/10.1046/j.1365-3040.1997.d01-104.x (1997).
33. Canham, C. D., Finzi, A. C., Pacala, S. W. & Burbank, D. H. Causes and consequences of resource heterogeneity in forests: interspecific variation in light transmission by canopy trees. *Can. J. Res.* **24**, 337–349. https://doi.org/10.1139/x94-046 (1994).
34. Guerrieri, R., Lepine, L., Asbjornsen, H., Xiao, J. & Ollinger, S. V. Evapotranspiration and water use efficiency in relation to climate and canopy nitrogen in US forests. *J. Geophys. Res. Biogeosci*. **121**, 2610–2629. https://doi.org/10.1002/2016JG003415 (2016).
35. Valladares, F. & Niinemets, Ü. Shade tolerance, a key plant feature of complex nature and consequences. *Annu. Rev. Ecol. Evol. Syst.* **39**, 237–257. https://doi.org/10.1146/annurev.ecolsys.39.110707.173506 (2008).
36. Knyazikhin, Y. et al. Reply to Townsend.: decoupling contributions from canopy structure and leaf optics is critical for remote sensing leaf biochemistry. Proc. Natl Acad. Sci. USA 110, E1075; (2013). https://doi.org/10.1073/pnas.1301247110
37. Burns, R. M. & Honkala, B. H. *Silvics of North America* Vol. 2 (US Department of Agriculture, Forest Service, 1990).
38. Canham, C. D. et al. Neighborhood analyses of canopy tree competition along environmental gradients in New England forests. *Ecol. Appl.* **16**, 540–554. https://doi.org/10.1890/1051-0761(2006)016[(2006). 0540:NAOCTC]2.0.CO;2.

39. LaRue, E. A. et al. Compatibility of aerial and terrestrial LiDAR for quantifying forest structural diversity. *Remote Sens.* **12**, 1407. https://doi.org/10.3390/rs12091407 (2020).
40. Atkins, J. W. et al. Application of multidimensional structural characterization to detect and describe moderate forest disturbance. *Ecosphere* **11**, e03156. https://doi.org/10.1002/ecs2.3156 (2020).
41. Jarvis, P. G. & McNaughton, K. G. Stomatal control of transpiration: scaling up from leaf to region. *Adv. Ecol. Res.* **15**, 1–49 (1986).
42. Brodribb, T. J. & Holbrook, N. M. Stomatal protection against hydraulic failure: a comparison of coexisting ferns and angiosperms. *New. Phytol*. **162**, 663–670. https://doi.org/10.1111/j.1469-8137.2004.01060.x (2004).
43. McDowell, N. et al. Mechanisms of plant survival and mortality during drought: why do some plants survive while others succumb to drought? New Phytol. **178**, 719–739 ; (2008). https://doi.org/10.1111/j.1469-8137.2008.02436.x
44. Martínez-Vilalta, J. & Garcia-Forner, N. Water potential regulation, stomatal behaviour and hydraulic transport under drought: deconstructing the iso/anisohydric concept. *Plant. Cell. Environ.* **40**, 962–976. https://doi.org/10.1111/pce.12846 (2017).
45. Comstock, J. P. & Mahall, B. E. Drought and changes in leaf orientation for two California chaparral shrubs: Ceanothus megacarpus and Ceanothus crassifolius. *Oecologia* **65**, 531–535. https://doi.org/10.1007/BF00379668 (1985).
46. Valladares, F. & Pearcy, R. W. Interactions between water stress, sun-shade acclimation, heat tolerance, and photoinhibition in the sclerophyll Heteromeles arbutifolia. *Plant. Cell. Environ.* **20**, 25–36. https://doi.org/10.1046/j.1365-3040.1997.d01-8.x (1997).
47. Smith, M. N. et al. Seasonal and drought-related changes in leaf area profiles depend on height and light environment in an Amazon forest. *New. Phytol*. **222**, 1284–1297. https://doi.org/10.1111/nph.15726 (2019).
48. Pearcy, R. W. & Sims, D. A. *Photosynthetic acclimation to changing light environments: scaling from the leaf to the whole plant in Exploitation of Environmental Heterogeneity by Plants* 145–174 (Academic, 1994).
49. Asner, G. P. Biophysical and biochemical sources of variability in canopy reflectance. *Remote Sens. Environ.* **64**, 234–253. https://doi.org/10.1016/S0034-4257(98)00014-5 (1998).
50. Hase, N. et al. Identifying the main drivers of the seasonal decline of near-infrared reflectance of a temperate deciduous forest. *Agric. Meteorol.* **313**, 108746. https://doi.org/10.1016/j.agrformet.2021.108746 (2022).
51. Hollender, C. A. & Dardick, C. Molecular basis of angiosperm tree architecture. *New. Phytol*. **206**, 541–556. https://doi.org/10.1111/nph.13204 (2015).
52. Weinstein, B. G. et al. Individual canopy tree species maps for the National Ecological Observatory Network. *PLoS Biol.* https://doi.org/10.1371/journal.pbio.3002700 (2024). 22, e3002700.
53. Almeida, D. R. A. et al. Optimizing the remote detection of tropical rainforest structure with airborne lidar: leaf area profile sensitivity to pulse density and spatial sampling. *Remote Sens.* **11**, 92.

https://doi.org/10.3390/rs11010092 (2019).

54. Rouse, J. W., Haas, R. H., Schell, J. A. & Deering, D. W. Monitoring vegetation systems in the Great Plains with ERTS. *NASA Spec. Publ.* **351**, 309 (1974).

55. Trabucco, A. & Zomer, R. Global Aridity Index and Potential Evapotranspiration (ET0) Climate Database v3. figshare; (2022). https://doi.org/10.6084/m9.figshare.7504448.v4

Figures

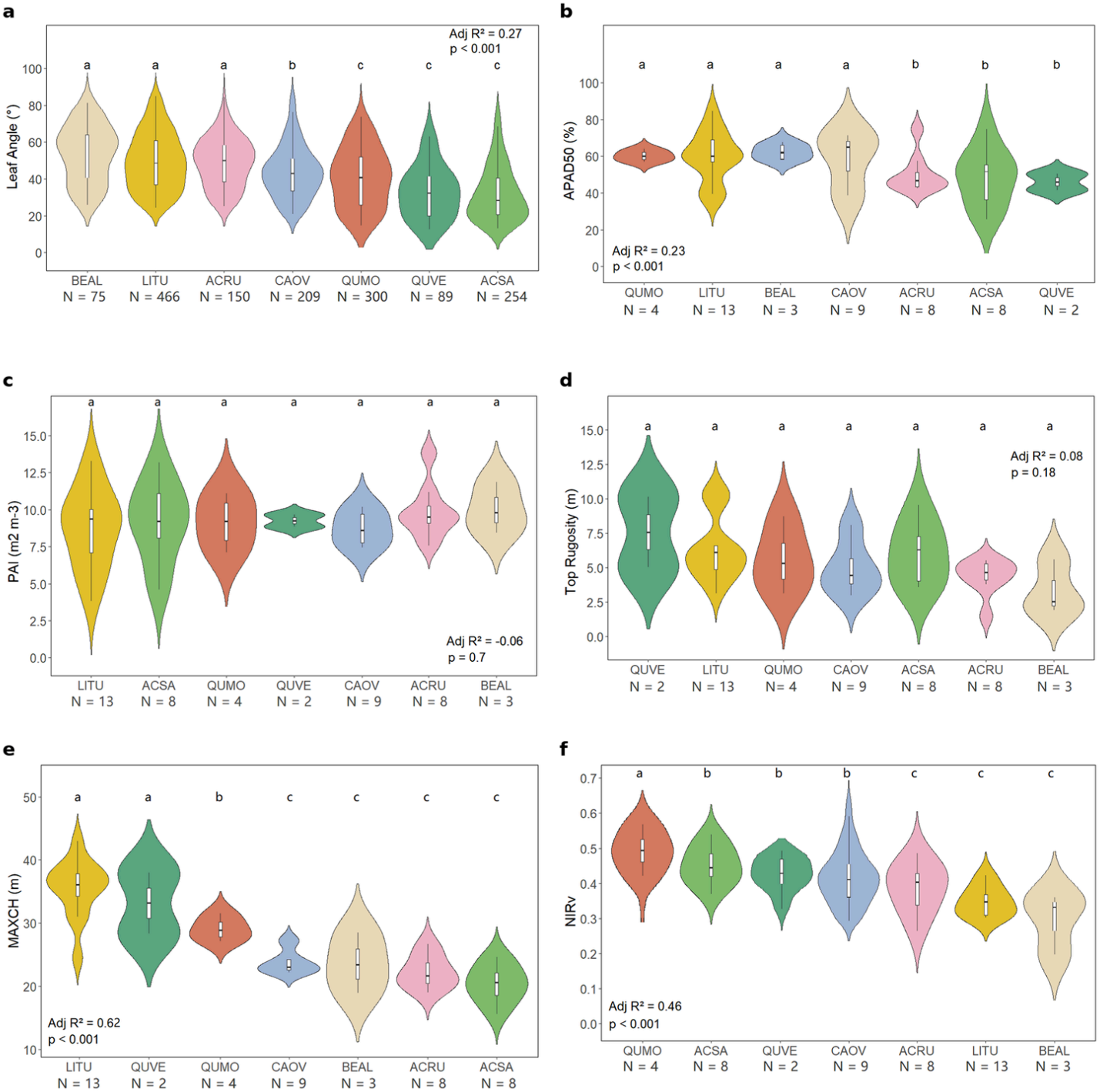

Figure 1

Interspecific variation in crown architectural traits and crown-scale NIR_V. Violin plots show distributions of (a) mean leaf angle, (b) accumulated plant area density in the upper half of the crown ($APAD_{50}$), (c) plant area index, (d) crown-top rugosity, (e) maximum canopy height and (f) near-infrared reflectance of vegetation (NIR_V). White boxes show the interquartile range and central lines show medians. For leaf angle, N is the number of measured leaves; for all other traits, N is the number of tree crowns measured for each species across all sites. Letters indicate Tukey HSD groups after one-way ANOVA. Adjusted R^2, F statistics and two-sided P values are shown for each panel.

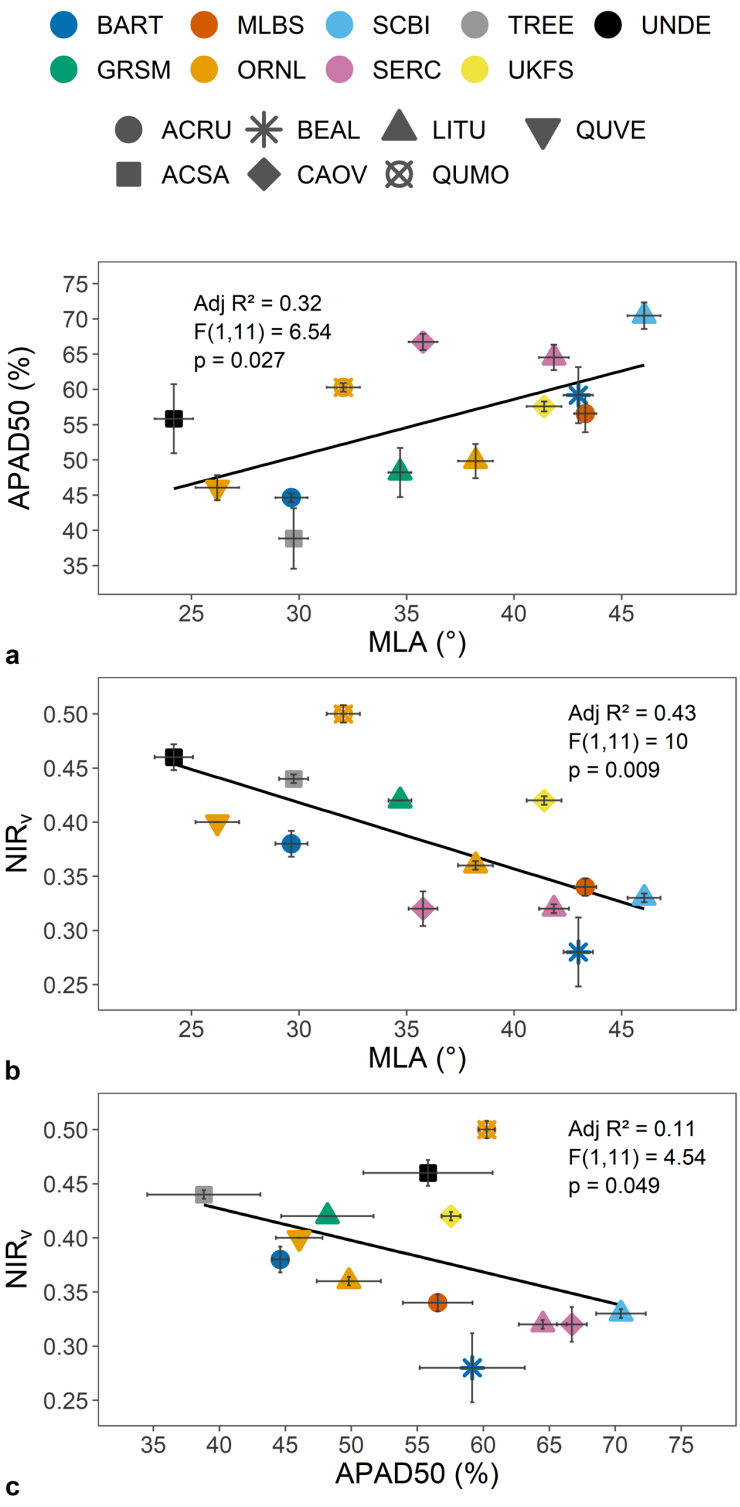

Figure 2

Key relationships within the summary dataset of measured tree species (symbols) and NEON sites (colors). Species names are in Table 1 and are listed here by species codes consisting of the first two letters of the genus and species (e.g. *Liriodendron tulipifera*, LITU). the RMA regression indicates that: in (a) trees have more vertical leaves (higher MLA) are on more top-heavy crowns (higher $APAD_{50}$); in (b) tree crowns with more vertical leaves are predictive of lower NIR_V; in (c) more top-heavy crowns (higher

$APAD_{50}$) are predictive of lower NIR_v. Points show site–species means and error bars show standard errors. Adjusted R^2, F statistics and two-sided P values are shown in each panel.

Supplementary Files

This is a list of supplementary files associated with this preprint. Click to download.

- FanetalScientificReportsSupplementaryInformation.pdf